ChemCatChem

Research Article
doi.org/10.1002/cctc.202500581

Chemistry Europe
European Chemical Societies Publishing

www.chemcatchem.org

Pd Nanoparticles Supported on Activated Carbon and Their Application in the Oxidative Condensation Reaction of Furfural: Effect of Base and Oxidizing Agent on Catalytic Behavior and Deactivation

Rocío Maderuelo Solera,[a, b] Eleonora Monti,[c, d] Ramón Moreno-Tost,[a, b] Cristina García-Sancho,[a, b] Pedro Maireles-Torres,[a, b] Juan Antonio Cecilia,*[a, b] and Nikolaos Dimitratos*[c, d]

Catalysts with different Pd loading (0.5–2 wt.%) supported on an activated carbon were synthesized and tested in the oxidative condensation reaction of furfural using absolute ethanol, sodium carbonate as base, and hydrogen peroxide as oxidizing agent. The characterization of the catalysts reveals a high dispersion of the Pd-species in the form of Pd^0. The catalytic results reported that furan-2-acrolein is the main product with a maximum yield of 52% after 6 h of reaction at 130 °C for the catalyst with the highest Pd content. To obtain this product, it is necessary to have the presence of an oxidant as hydrogen peroxide, to promote the oxidation of ethanol to acetaldehyde, and then a base, which promotes its condensation reaction with the furfural molecule. The progressive decay of the furan-2-acrolein yield and the conversion values after several cycles suggests the formation of carbonaceous deposits on the surface of the catalysts, which block the metallic sites involved in the reactions, as was observed by X-ray photoelectron spectroscopy and CO-chemisorption studies.

1. Introduction

The industrial production of furfural (FUR) started in 1921 by Quaker Oats Company from the treatment of corn cobs, oat hulls and sugar cane bagasse. Initially, the demand of FUR was very limited;[1] however, the world market has increased significantly in the last decades since this molecule has been considered as a building block chemical.[2,3] FUR is used as a solvent to extract aromatics from diesel fuels, wax, vegetable, or lubricating oils. Other applications as a solvent include the manufacture of phenolic resins or the extraction of butadiene.[4] However, the main interest of FUR is attributed to its high reactivity since both the furan ring and the aldehyde group of this molecule present high reactivity such that it is possible to obtain a wide range of molecules with high added value.[2,3,5] About 70% of the obtained FUR is employed in the synthesis of furfuryl alcohol from a hydrogenation reaction.[5,6] The interest of this compound lies in its high thermochemical stability in the polymer field.[7] Other valuable compounds with lower demand, used as fuel additives, fine chemistry, fragrances or pharmaceutical field, can also be obtained from FUR although in smaller proportions.

Focusing on the valorization of FUR through oxidation processes, several reviews have reported the synthesis of valuable compounds such as maleic anhydride, maleic acid, succinic acid, furanones, furoic acid, and alkyl furoates, among others.[8,9] Industrially, the direct oxidation of the aldehyde group to obtain furoic acid takes place through the Cannizzaro reaction, where FUR is subjected to a dismutation reaction, obtaining furfuryl alcohol and furoic acid, although the yield toward these products is limited to a maximum value of 50%.[10] Some authors have pointed out that the amount of furonic acid can be improved with the use of a sacrificial aldehyde as formaldehyde.[8]

The use of alcohol in the reaction medium can involve consecutive reactions such as oxidative esterification to obtain alkyl furoates or oxidative condensation to form furan-2-acrolein derivatives.[8] Both reactions give rise to high-added value products since precursors of polymers or resins, fragrances, flavors, or fine chemical compounds used in the creation of chemical

[a] R. M. Solera, Dr. R. Moreno-Tost, Dr. C. García-Sancho, Prof. P. Maireles-Torres, Prof. J. A. Cecilia
Departamento de Química Inorgánica, Cristalografía y Mineralogía, Facultad de Ciencias, Universidad de Málaga, Campus de Teatinos, Málaga 29071, Spain
E-mail: jacecilia@uma.es

[b] R. M. Solera, Dr. R. Moreno-Tost, Dr. C. García-Sancho, Prof. P. Maireles-Torres, Prof. J. A. Cecilia
Instituto de Biorrefinerías "I3B", Universidad de Málaga, Campus de Teatinos, Málaga 29071, Spain

[c] Dr. E. Monti, Prof. N. Dimitratos
Dipartimento di Chimica Industriale "Toso Montanari", Università di Bologna, Viale Risorgimento 4, Bologna 40136, Italy
E-mail: nikolaos.dimitratos@unibo.it

[d] Dr. E. Monti, Prof. N. Dimitratos
Center for Chemical Catalysis—C3, Alma Mater Studiorum, Università di Bologna, Viale Risorgimento 4, Bologna 40136, Italy

Supporting information for this article is available on the WWW under https://doi.org/10.1002/cctc.202500581

sensors, photoactive molecules, or in organic electron transfer systems due to their chemical structure promote interactions that involve electron transfer or photo-induced reactions.[8]

Several studies have reported that the use of short-chain alcohol, such as methanol, acts reactive/solvent, promoting oxidative esterification to form methyl furoate as the main product.[8] Generally, this reaction takes place with the use of Au-based catalysts, although the effect of the support has an important role in the catalytic behavior, obtaining the highest yields when TiO_2, CeO_2, ZrO_2, or MgO are used as the desired support.[11–14] In the last years, some authors have also reported that the use of small Co-nanoparticles also promotes the oxidative esterification of FUR.[15,16]

The oxidative condensation of FUR takes place with primary or secondary alcohols, which are oxidized in the reaction medium to form their respective aldehyde or ketones. Then, a base extracts hydrogen in the α-position of the carbonyl group, promoting the oxidative condensation with the carbonyl group of the FUR to form furan-2-acrolein derivatives.[8] The majority of the studies have been performed with Au-based catalysts,[17–19] although other active catalysts as Pt,[20] Pd,[21–23] CoO_x,[24] CuO[25–27] have also been explored. On the other hand, some studies have reported that the presence of Pd species also gives rise to C—C coupling reactions.[28–30]

Generally, these catalysts reach high conversion values, although the presence of a base, which promotes condensation reactions, leads to uncontrolled reactions and the formation of humins. In this study, Pd-species have been dispersed on an activated carbon. The main novelty of the present manuscript is focused on how the textural properties, as well as the surface of the catalyst and the active phase, are affected by the deposition of these humins, due to the uncontrolled condensation reactions. The characterization of the used catalysts was correlated with the decay of the conversion and yield values in the oxidative condensation of FUR into furan-2-acrolein.

2. Results and Discussion

2.1. Characterization of the Catalysts

The crystallinity of the support and the catalyst with the highest Pd-content, that is, 2 wt.% Pd/AC, was evaluated by XRD analysis (Figure 1). In both cases, two broad diffraction peaks presented at 2θ (°) of 24.4 and 43.3 were observed. The first diffraction peak is attributed to the d002 reflection, whereas the diffraction peak presented at higher 2θ value is assigned to the overlapping of the d101 and d100 reflections of a graphitic carbon with poor ordering (PDF:41-1487).[31] On the other hand, other diffraction peaks were also observed. These signals are attributed to the existence of SiO_2 as impurities (PDF: 01-078-4811). Finally, the presence of diffraction peaks assigned to Pd-species must be ruled out due to the low proportion of Pd-incorporated and/or high dispersion.

The morphology of the catalysts, as well as the arrangement of Pd nanoparticles by STEM and elemental analysis, is presented (Figure 2). The micrographs reveal a high dispersion of the Pd

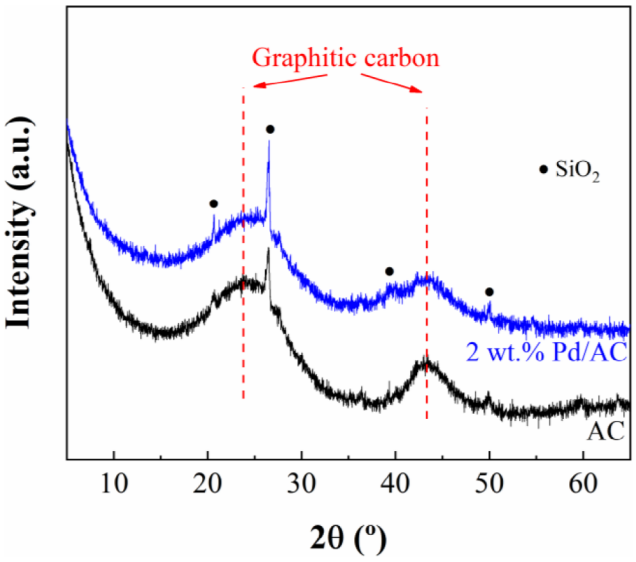

Figure 1. X-ray diffraction of the activated carbon (AC) and the catalyst with the highest Pd-content (2 wt.% Pd/AC).

nanoparticles with spherical morphology. Despite the increase in Pd loading, the particle size of the Pd nanoparticles appears to be similar in all catalysts, with particle diameters less than 3 nm in most cases. This confirms the potential of the synthesis strategy to synthesize small Pd nanoparticles with a high degree of dispersion. A detailed analysis of the particle size distribution of the Pd nanoparticles confirms high homogeneity in all catalysts (Figure 3). In fact, the maximum of the histograms is very similar in all cases since 0.5 wt.% Pd/AC catalyst and 1 wt.% Pd/AC catalyst shows maxima at 1.38 and 1.39 nm, respectively, whereas the 2 wt.% Pd/AC catalyst shows a maximum at a slightly lower value (0.95 nm). These data confirm the formation of Pd-based catalysts, with a small mean Pd particle size and narrow particle size distribution, suggesting a high dispersion of the active phase onto the support.

The determination of the textural properties was carried out from their N_2 adsorption–desorption isotherms at −196 °C (Figure S1, Supporting Information) as well as the CO_2 adsorption–desorption isotherms at 0 °C (Figure S2, Supporting Information). The analysis of the N_2 adsorption–desorption profiles at −196 °C reveals that both support and catalysts adsorb a high amount of N_2 at low relative pressure, suggesting the presence of high microporosity in these samples.[32] Moreover, the presence of a very narrow hysteresis loop also confirms the presence of a pore diameter less than 4 nm.[32] Likewise, the samples also adsorb a high proportion of N_2 at high relative pressure, which must be ascribed to the voids between adjacent particles of activated carbon.[32] The estimation of the textural properties (Table 1) shows in what manner the surface area progressively decreases when an increasing number of Pd-species are incorporated on the support, reducing the surface area of the support from 1146 to 898 m^2/g for 2 wt.% Pd/AC sample, as an example. Furthermore, the estimation of the microporosity by the t-plot method[32] confirms that the support is highly microporous. In the same way, these data also indicate that the incorporation of

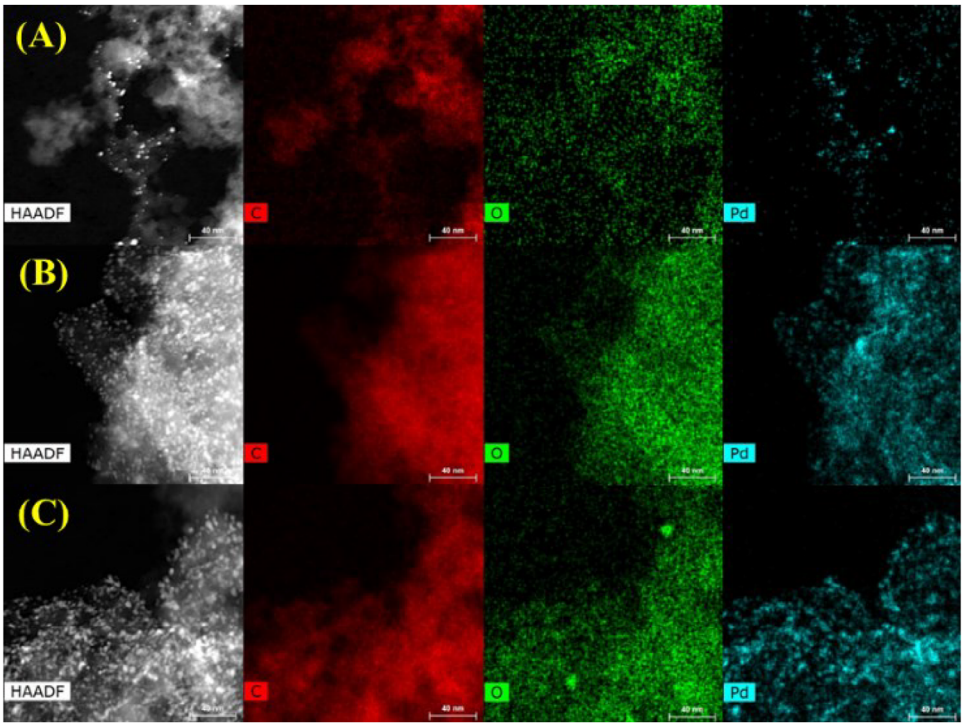

Figure 2. STEM micrographs and elemental analysis of 0.5 wt.% Pd/AC (A), 1 wt.% Pd/AC (B) and 2 wt.% Pd/AC (C). Scale 40 nm.

Pd-species causes a slight blockage of the micropores while the meso- and macropores hardly suffer modifications. The analysis of the pore volume is in agreement with the data from the analysis of the surface area, since the pore volume diminishes when the Pd-species are incorporated because of the blockage of the micropore.

Previous studies have established that the use of N_2 as a target molecule to determine the porosity is not entirely appropriate for the determination of the porosity in narrow micropores because N_2 cannot easily access these small pores.[33] However, the CO_2-adsorption isotherm is carried out at a higher temperature than N_2-adsorption (0 °C versus −196 °C), which favors the diffusion of this molecule in small micropores, as those presented in activated carbon generally are. Similarly, the higher quadrupole moment of the CO_2 molecules also promotes a better interaction with the narrow micropore, such that it is easier to reach equilibrium conditions at low pressure values.[33,34] Therefore, the microporosity was also determined by the Dubinin–Radushkevich equation.[35] The results reported in Table 2 confirm that support and catalysts are highly microporous. Likewise, the progressive incorporation of Pd nanoparticles causes a decrease in the surface area and the micropore volume due to the Pd nanoparticles must block the pore partially. These data follow the same trend as with the data observed when the N2 molecule was used as the reference molecule.

Considering the high microporosity of the materials and according to TEM micrographs (Figure 2), Pd nanoparticles are deposited on the surface of the activated carbon, causing a partial blockage of its micropores. Furthermore, the micropore is so narrow that TEM micrographs do not have enough resolution to detect this porosity. Given the analysis of the textural properties, it is likely that most of these narrow micropores are too small for the FUR molecule to access these regions. Therefore, the reaction must take place on the surface of the catalysts.

The determination of the metallic Pd sites involved in the reaction was determined from CO chemisorption analysis (Table 3). The quantification of these sites was carried out assuming that each active site interacts with one CO molecule. The data reported show how the metallic surface per gram of sample increases with the gradual increase of the amount of Pd nanoparticles deposited on the surface of AC. However, it is striking how the analysis of the metallic surface per gram of metal displays similar values (105–112 m^2/g of metal). These data reveal that the particles are homogeneous and that they are also highly dispersed (23.5%–25.1%), which is in agreement with the data shown from the TEM micrographs, where the particle size of Pd was similar in all cases. In the same way, the determination of the active sites reveals a quasi-linear increase of the CO chemisorption values with the Pd-content from 11 μmol/g for 0.5 wt.% Pd/AC catalyst to 46 μmol/g for 2 wt.% Pd/AC catalyst, which is directly related to the high dispersion and homogeneity of the Pd nanoparticles.

The chemical composition on the surface of the catalysts, as well as the dispersion, was analyzed by XPS (Table 4 and Figure 4). The analysis of the C 1s core level spectra of the catalysts (Figure 4A) displays three contributions. The main contribution located about 284.8 eV is attributed to the overlapping of adventitious carbon, C—C bonds, and C═C bonds. The contribution located about 286.1 eV is assigned to —C—O bonds, while the signal located at 287.3 eV is ascribed to —C═O bonds.[36] The analysis of the O 1s core level spectra also shows three

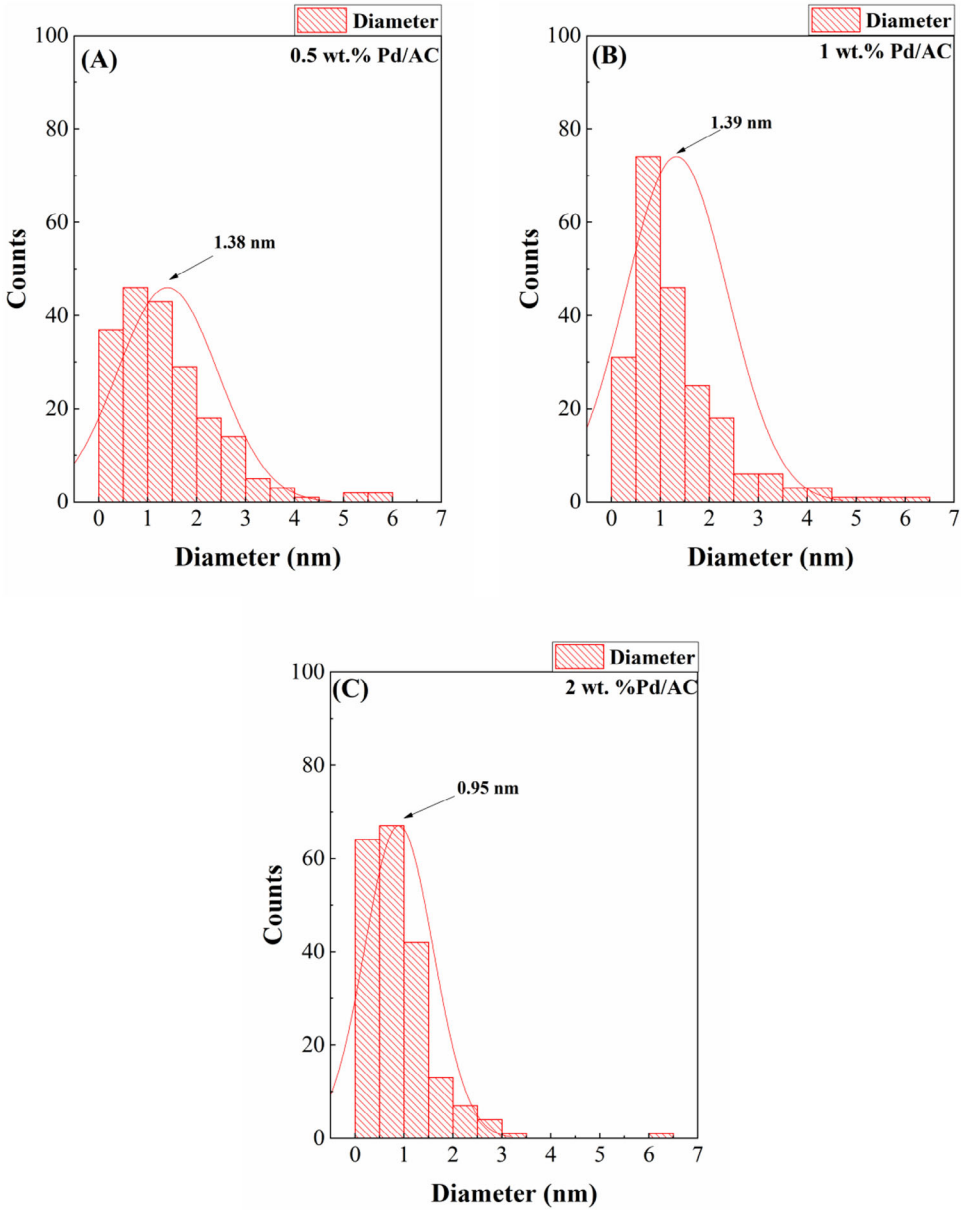

Figure 3. Histograms of the particle diameter for the Pd-species in 0.5 wt.% Pd/AC (A), 1 wt.% Pd/AC (B) and 2 wt.% Pd/AC (C) catalysts. Number of measured particles: 200 counts.

Table 1. Determination of the textural properties of the activated carbon and Pd-based catalysts from the N_2 adsorption–desorption isotherms at −196 °C.

Samples	Langmuir Surface (m^2/g)	t-Plot (m^2/g)	S_{ext}(m^2/g)	Pore Volume (cm^3/g)	Micropore Volume (cm^3/g)
AC	1146	876	237	0.6750	0.2647
0.5 wt.% Pd/AC	1049	798	250	0.6219	0.2410
1 wt.% Pd/AC	982	738	243	0.5874	0.2207
2 wt.% Pd/AC	898	627	230	0.5441	0.2085

contributions (Figure 4B). The contribution located at the lowest value of binding energy (532.2 eV) is assigned to C═O bonds. The contribution located at intermediate binding energy (533.8 eV) is attributed to C—O bonds, while the smaller contribution located at the highest binding energy value (536 eV) is assigned to —C—O—H bonds.[36] Regarding the analysis of the Pd 3d core level spectra (Figure 4C), two contributions are observed for the Pd $3d_{5/2}$ region. The main contribution located at about 336 eV is assigned to the presence of Pd^0-species, while the lower contribution, which appears at about 338 eV, is attributed to

Table 2. Determination of the textural properties of the activated carbon and Pd-based catalysts from the CO_2 adsorption–desorption isotherms at 0 °C

Catalysts	Surface (m^2/g)	Limiting Pore Volume (cm^3/g)
AC	603	0.2420
0.5 wt.% Pd/AC	576	0.2310
1 wt.% Pd/AC	539	0.2164
2 wt.% Pd/AC	475	0.1924

Table 4. Atomic concentrations on the surface of the catalysts, estimated by XPS, of 0.5 wt.% Pd/AC, 1 wt.% Pd/AC, and 2 wt.% Pd/AC catalysts.

Catalyst	Atomic Surface Concentrations (%)				
C 1s	O 1s	Pd 3d	Na 1s	Cl 2p	
0.5 wt.% Pd/AC	80.77	16.09	0.45	2.39	0.30
1 wt.% Pd/AC	79.77	16.82	1.03	2.10	0.27
2 wt.% Pd/AC	76.74	19.66	1.95	1.73	0.19

the presence of Pd^{2+}-species. These data indicate that a small proportion of Pd after complete chemical reaction is partially oxidized during the handling step.[36] Hence, the catalyst with the lowest Pd-content displays about 30% in the form of Pd^{2+} while the catalyst with the highest content only shows a 9% of Pd^{2+}-species.

The analysis of the surface chemical composition of the catalysts (Table 4) confirms that the catalysts are highly carbonaceous, while the oxygen content depends on the temperature of the thermal activation of the commercial AC. The Pd content on the surface of the catalysts is directly related to the amount of Pd deposited, ranging from 0.45% to 1.95%. These values are in good agreement with the data obtained by ICP, where the Pd content is 0.55%, 1.10%, and 2.04% for 0.5 wt.% Pd/AC, 1 wt.% Pd/AC and 2 wt.% Pd/AC, respectively. In both cases, the obtained values are very close to the theoretical data due to the high dispersion and particle size of the Pd-species, as was observed in Figures 2 and 3 and Table 3. In addition, small impurities of Na and Cl are also observed. These impurities could be ascribed to the experimental process used for the chemical reduction of Pd^{2+}-species and the use of $NaBH_4$ as reducing agent. Finally, it is interesting that Si-species are not observed although SiO_2 was detected by XRD analysis. It is possible that the AC can have small impurities of SiO_2 in the form of quartz with a high degree of crystallinity.

2.2. Catalytic Tests

Once the Pd nanoparticles supported on AC were characterized, these samples were tested in the oxidative condensation of FUR using absolute ethanol, Na_2CO_3 as the chosen mild base, and H_2O_2 as an oxidizing agent (Scheme 1).

In the first study, the influence of the reaction temperature on the catalytic behavior was studied (Figure 5). The catalytic tests after 6 h of reaction show how an increase in temperature improves the FUR conversion. Figure 5 also shows that the sample without the presence of Pd (only AC) displays some activity with a maximum conversion of 15%, which is in agreement with other reported studies.[22] Both results suggest that the reaction conditions have a positive effect on the oxidative condensation of FUR. Nevertheless, the presence of Pd has a notable effect in terms of catalytic performance, since the highest FUR conversion is obtained for 2 wt.% Pd/AC catalyst, reaching a maximum value of 95% after 6 h of reaction at 150 °C. Regarding the obtained products, furfuryl alcohol (FOL), furan-2-acrolein (F2A), and difuryl-methane (DFM) are detected in all cases. The presence of FOL is relatively low for all reaction temperatures, reaching yields below 10% in all cases, although these values slightly increase for catalysts with higherPd contentt. The obtained results reveal that the maximum yield is toward F2A, reaching a maximum value of 52% when the reaction occurs at 130–140 °C for 6 h for the 2 wt.% Pd/AC catalyst. This value is slightly higher than that reported in the literature for a Pd-based catalyst supported on an activated carbon with the presence of acid sites, which are promoted by the presence of Pd-species in the activation, achieving a maximum F2A yield of 44% at a higher temperature (150 °C).[39] DFM was also obtained, although in a lower amount, being more noticeable at higher temperatures. Finally, all catalysts show the presence of a high amount of non-detected (ND) products, mainly at higher temperatures. During the progress of the reaction, the development of a dark color is evident, suggesting the formation of humins. Humins are formed due to the high reactivity of furfural to an oxidizing and aqueous medium by the formation of H_2O during the hydrogen peroxide decomposition, favoring uncontrolled polymerization reactions.

In order to evaluate the role of acetaldehyde formation in the oxidative condensation of furfural, an additional test was carried out, taking into consideration the maximum yield toward F2A (130 °C/6 h/2 wt.% Pd/AC catalyst) by replacing ethanol with acetaldehyde and using the same concentration. This study reported that F2A yield is 72% when acetaldehyde is added to

Table 3. Determination of the dispersion, metallic area, and CO chemisorption for the Pd-based catalysts supported on AC.

Sample	Dispersion (%)	Metallic Area (m^2/g of sample)	Metallic Area (m^2/g of metal)	CO Chemisorption (μmol/g)
0.5 wt.% Pd/AC	25.1	0.55	112	11
1 wt.% Pd/AC	23.5	1.05	105	22
2 wt.% Pd/AC	24.3	2.20	110	46

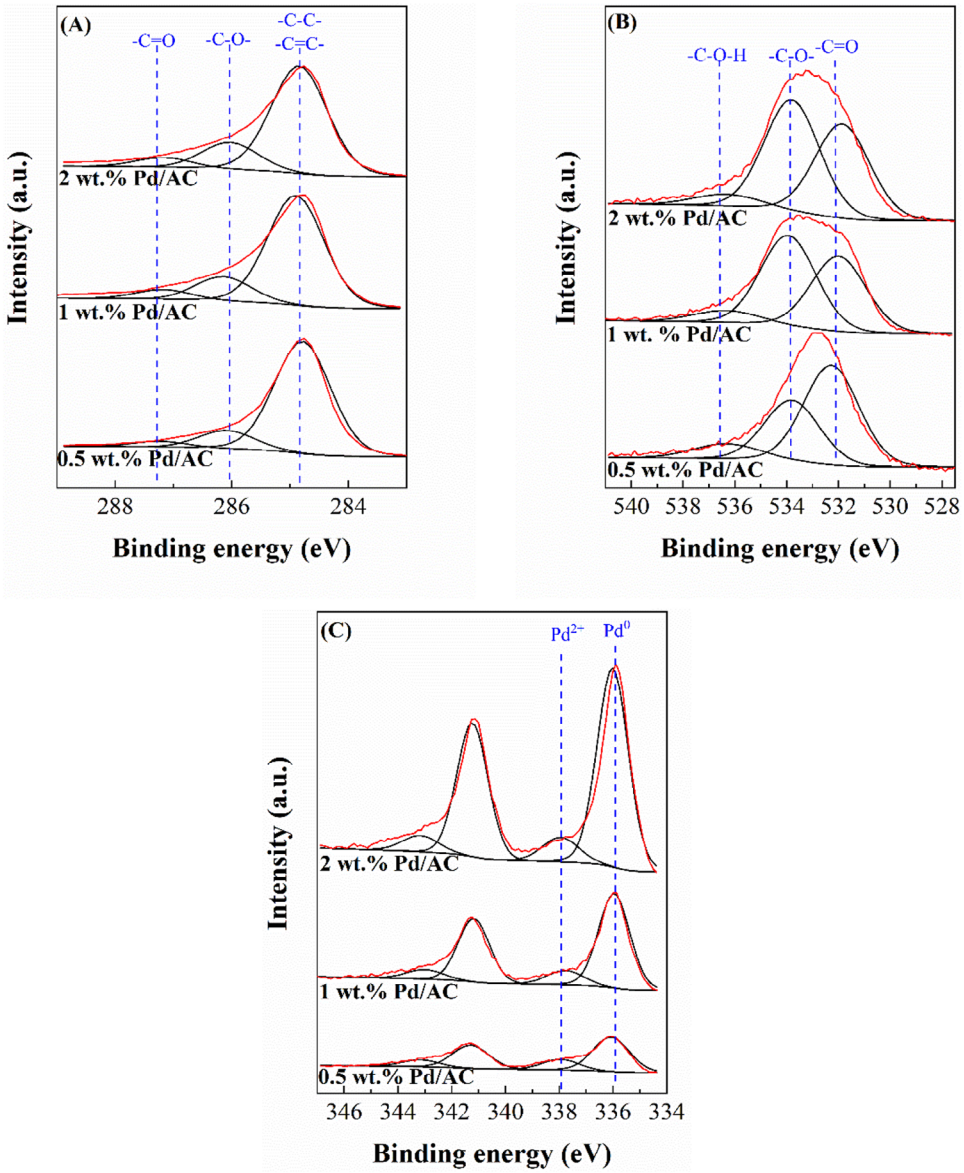

Figure 4. C 1s (A), O 1s (B), and Pd 3d (C) core level spectra of 0.5 wt.% Pd/AC, 1 wt.% Pd/AC, and 2 wt.% Pd/AC catalysts.

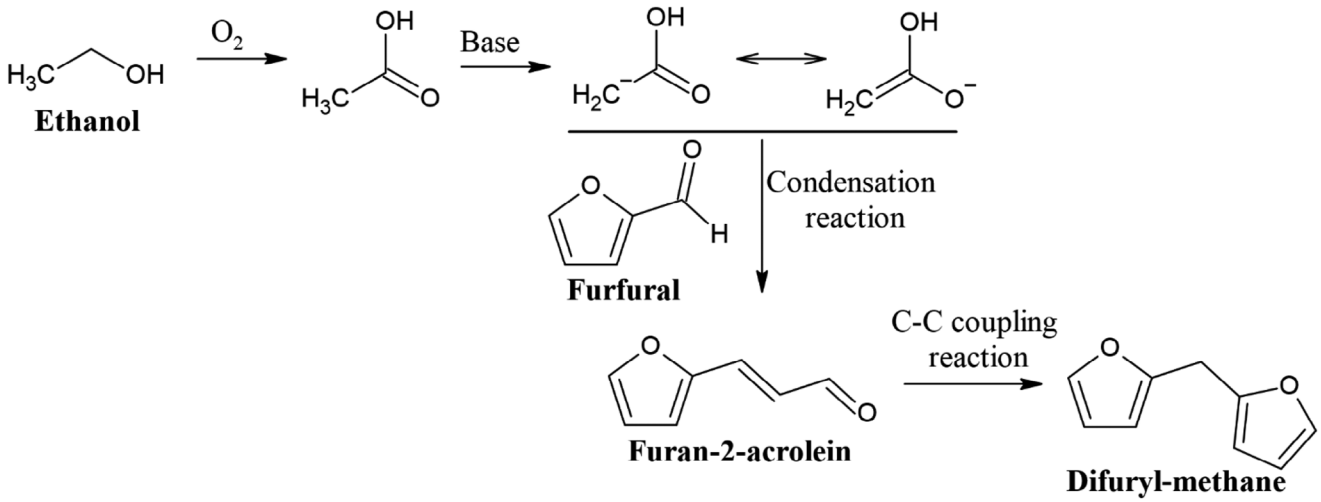

Scheme 1. Proposed reaction mechanism of the oxidative condensation of furfural according to the literature.[20–24]

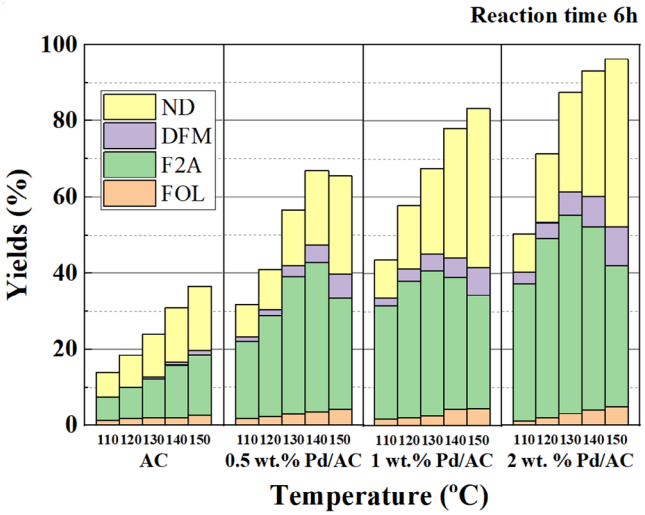

Figure 5. Conversion and yields at different reaction temperatures in the oxidative condensation of FUR using Pd/AC catalysts. (Experimental conditions: catalyst loading = 0.05 g; amount of FUR = 1 mmol; volume of absolute ethanol = 5 mL; Na_2CO_3 amount = 0.10 g; and H_2O_2 (33 vol. %) volume = 0.5 mL; reaction temperature = 110–150 °C; reaction time = 6 h).

the reaction medium, while, in the case of using ethanol leads to a F2A yield of 52%. These data confirm that the formation of acetaldehyde limits the oxidative condensation of FUR to form F2A.

Regarding the mechanism of the obtained products (Scheme 1), FOL can be obtained from two different pathways. The first pathway shows that FUR could be subjected to the Cannizzaro reaction, where a base induces the disproportionation into a primary alcohol (FOL) and a carboxylic acid (furoic acid). However, this acid was not detected; therefore, this route must be ruled out.[8] On the other hand, ethanol can promote hydride transfer to form FOL, although this alcohol can be partially oxidized by the presence of oxidizing medium, giving rise to cyclical reaction.[8,37] The formation of the main product (F2A) takes place through several consecutive reactions. First, the alcohol used as a solvent, but at the same time as a reagent, is oxidized to its respective aldehyde.[21–23] In this case, previous studies have reported that H_2O_2 reacts on the surface of Pd nanoparticles, adsorbing ·OH radicals, which display a higher redox potential than those shown for O_2 molecules.[38] The data reported in Figure 5 confirm that the presence of Pd-nanoparticles has a positive effect on the catalytic behavior. Thus, the presence of low Pd loading (0.5 wt.%) appears to be sufficient to promote the initial oxidation of ethanol to acetaldehyde.[17,20,21] In a second step, the presence of a base promotes the formation of an enolate that favors the formation of aldol condensation reactions.[20,21,24] On the other hand, the formation of DFM occurs by the C—C coupling reaction of F2A through Pd-based catalysts.[23,40,41] Finally, all catalysts show the presence of a high amount of non-detected products, mainly at higher reaction temperatures. As we have mentioned previously, this reaction gives rise to rather dark reaction media, suggesting the formation of humins, which are formed due to the high reactivity of furfural in an oxidizing and aqueous medium by the formation of H_2O during the hydrogen peroxide decomposition, favoring uncontrolled polymerization reactions. In the same way, the aldol condensation reaction of FUR and acetaldehyde under these catalytic conditions also gives rise to a wide range of uncontrolled condensation reactions.[37]

As the catalytic data in Figure 5, the highest yields toward F2A are obtained at 130 °C. Therefore, this temperature was selected for further kinetic studies. The conversion data, presented in Figure 6, demonstrate that all Pd-based catalysts follow a similar trend, increasing the FUR conversion along the reaction time for all catalysts. However, the conversion values differ between them since the activity is directly correlated as a function of the Pd content. Thus, 0.5 wt.% Pd/AC reaches a FUR conversion of 65% while 2 wt.% Pd/AC achieves a conversion of 94% after 24 h of reaction at 130 °C.

Regarding the yields of products, the main product is F2A, increasing its value as a function of the reaction time, while the yield of FOL is below 5% in all cases. As it was indicated previously, the F2A product is obtained in two steps. Firstly, the oxidation of ethanol into acetaldehyde and, secondly, the condensation of acetaldehyde with FUR. However, as shown in Figure 6, this yield begins to decrease after 6 h of reaction at 130 °C. In this way, the reaction profile of all Pd-based catalysts shows how the decrease of F2A is directly related to the formation of DFM, which is formed through a coupling reaction between two F2A molecules. On the other hand, FOL is also detected in a very low proportion. This product is formed through a reduction reaction. Considering the oxidizing environment of the reaction, very low yield values toward FOL are expected. Finally, the levels of non-detected products increase progressively along the reaction time. This increase is more pronounced in the case of the most active catalysts, that is, the catalyst with the highest Pd content. The oxidizing environment of the reaction and the presence of highly reactive molecules such as FUR, FOL, and F2A promote uncontrolled polymerization and condensation processes.

As the number of active sites per gram of catalyst was estimated from the CO chemisorption studies (Table 3), it is possible to determine the amount of F2A obtained per gram of catalyst and active site, that is, the productivity (Figure 7). The study was carried out at short reaction times, where the mol of F2A converted per gram and active site increases linearly as a function of reaction time. This linearity is lost at longer reaction times due to the depletion of the FUR molecules and/or partial blocking of the active sites. Considering these premises, the catalyst with the highest productivity is 0.5 wt.% Pd/AC with a value of 252 h^{-1}, while the least productive catalyst is 2 wt.% Pd/AC, which shows a value of 75 h^{-1}.

As indicated above, the oxidative condensation of FUR requires an oxidizing medium to carry out the reaction. Therefore, the amount of H_2O_2 was varied to further analyze and evaluate the role of oxidizing power in the following study (Figure 8). Catalytic conversion data ranges from 68 to 87% when the reaction takes place at 130 °C for 6 h. However, the most noticeable feature is the progressive variation of the reaction product profile by varying the H_2O_2 amount. Therefore, the catalytic assay without H_2O_2 shows high levels of FOL, with a

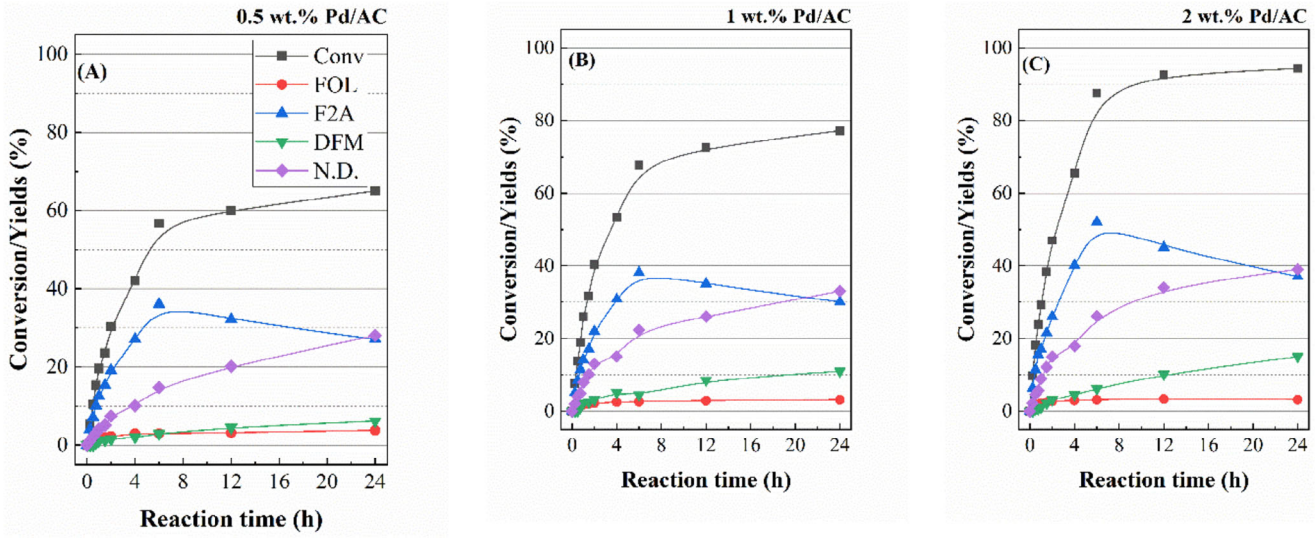

Figure 6. Conversion and yields at different reaction temperatures in the oxidative condensation of FUR using Pd/AC catalysts. (Experimental conditions: catalyst loading = 0.05 g; amount of FUR = 1 mmol; volume of absolute ethanol = 5 mL; Na_2CO_3 amount = 0.10 g; and H_2O_2 (33 vol. %) volume = 0.5 mL; reaction temperature = 130 °C; reaction time = 0–24 h).

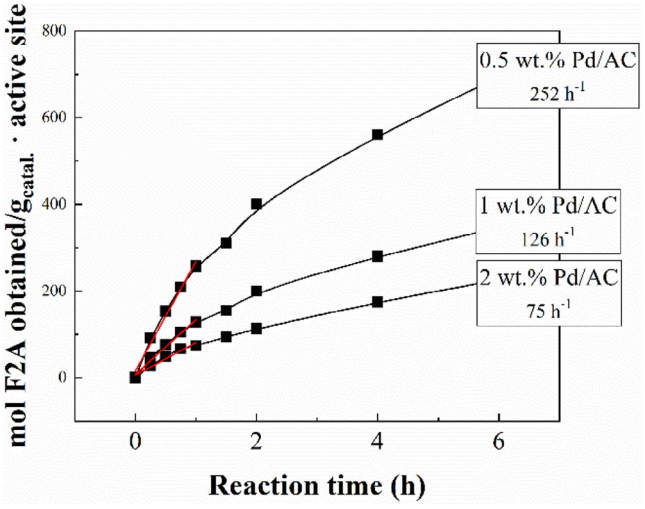

Figure 7. Determination of the TOF values for Pd-based catalysts supported on AC. (Experimental conditions: catalyst loading = 0.05 g; amount of FUR = 1 mmol; volume of absolute ethanol = 5 mL; Na_2CO_3 amount = 0.10 g; and H_2O_2 (33 vol. %) volume = 0.5 mL; reaction temperature = 130 °C; reaction time = 0–6 h).

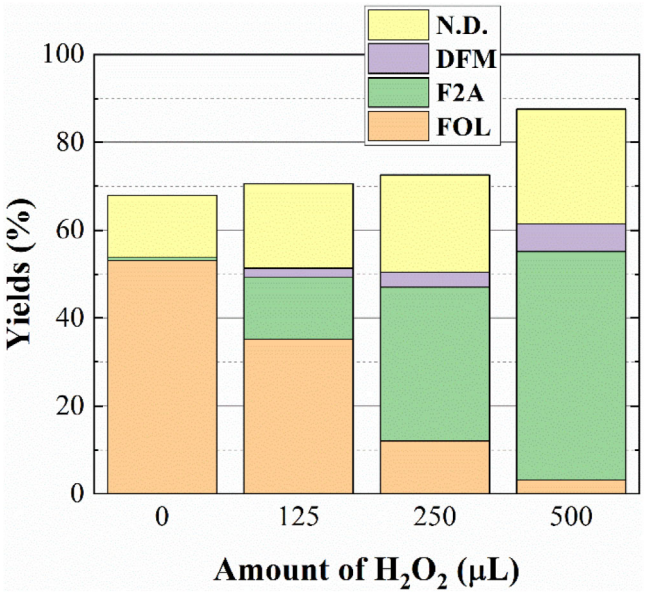

Figure 8. Influence of the addition of H_2O_2 in the reaction medium for the 2 wt.% Pd/AC catalyst. (Experimental conditions: catalyst loading = 0.05 g; amount of FUR = 1 mmol; volume of absolute ethanol = 5 mL; Na_2CO_3 amount = 0.10 g; and H_2O_2 (33 vol. %) volume = 0–0.5 mL; reaction temperature = 130 °C; reaction time = 6 h).

yield of 53% after 6 h of reaction at 130 °C. This data reveals that the absence of an oxidizing medium promotes the FUR reduction reaction. These results are in agreement with previous studies carried out using Pd-based catalysts. These studies have reported the hydrogenation of FUR to FOL using a hydrogenating agent, such as pressurized H_2 or an alcohol, which acts as a hydrogen donor.[42,43] These data suggest that in the absence of an oxidizing medium, the prevention of the oxidation of ethanol to acetaldehyde is carried out, which is necessary to promote the condensation reaction with FUR under a basic medium. The progressive addition of an oxidant agent, such as H_2O_2, to the reaction medium causes a decrease in FOL yield, which is accompanied by an increase in F2A levels. This implies that the addition of 500 μL of H_2O_2 generates a reaction medium, which is sufficiently oxidizing, to promote the oxidation of ethanol into acetaldehyde to take place and consequently to facilitate, in a following step under a basic medium, a condensation reaction. However, the presence of this oxidizing medium also causes an increase in the levels of non-detected products because the formation of a higher amount of acetaldehyde promotes condensation with FUR to form F2A although other undesired condensation reactions can also take place, therefore it is important to control the concentration of H_2O_2 used for promoting

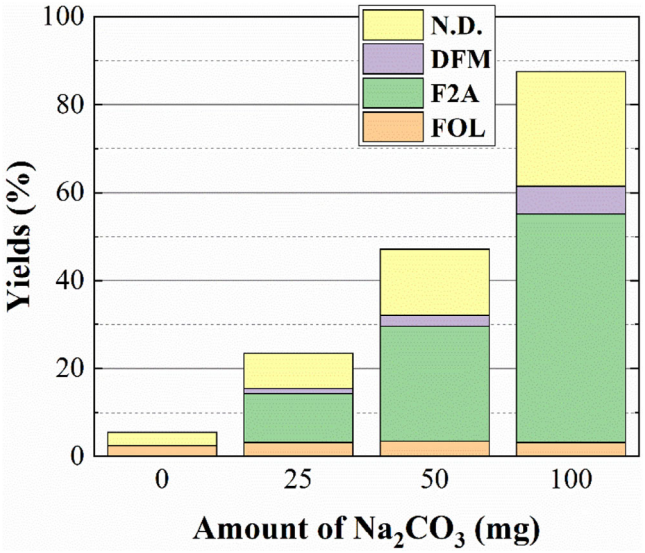

Figure 9. Influence of the addition of Na_2CO_3 in the reaction medium for the 2 wt.% Pd/AC catalyst. (Experimental conditions: catalyst loading = 0.05 g; amount of FUR = 1 mmol; volume of absolute ethanol = 5 mL; Na_2CO_3 amount = 0–0.10 g; and H_2O_2 (33 vol. %) volume = 0.5 mL; reaction temperature = 130 °C; reaction time = 6 h).

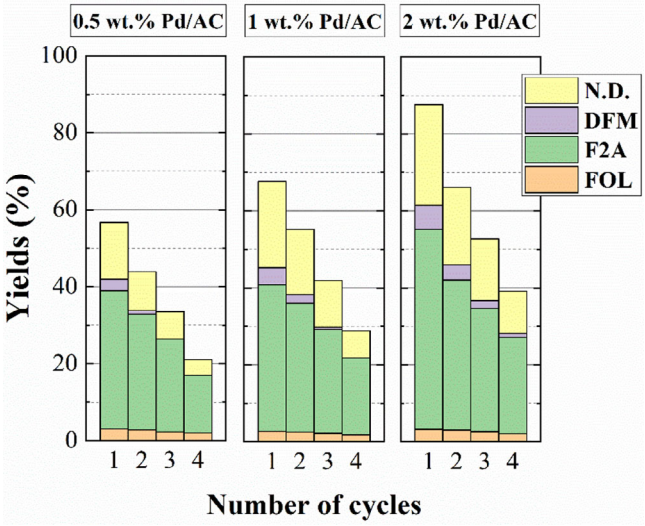

Figure 10. Reuse studies of the Pd-based catalysts supported on AC. (Experimental conditions: catalyst loading = 0.05 g; amount of FUR = 1 mmol; volume of absolute ethanol = 5 mL; Na_2CO_3 amount = 0–0.10 g; and H_2O_2 (33 vol. %) volume = 0.5 mL; reaction temperature = 130 °C; reaction time = 6 h).

the desired reaction and minimizing the formation of undesired products.

In the following study, the role of the amount of base in the oxidative condensation reaction was also studied (Figure 9). Previous studies have determined that the strength of the base plays a determining role in this reaction since a very weak base hardly promotes the condensation reaction between acetaldehyde and FUR.[23] In contrast, the use of a very strong base such as NaOH results in complete conversion. However, the condensation reactions are uncontrolled and therefore form a significant amount of humins, and therefore the undetected levels of byproducts are very high and leading to deactivation of catalysts.[23] The results reported in Figure 9 show how the presence of base has a clear influence in terms of catalytic behavior. The reaction without base barely has any catalytic conversion, reaching a conversion below 6% with selectivity toward F2A. The progressive addition of base causes an improvement in catalytic behavior. Regarding the products obtained, the yield toward FOL is similar in all tests, suggesting that the amount of base does not seem to have a strong influence on the formation of this product under the studied experimental conditions. The increase in the conversion of FUR is directly related to the formation of F2A since the amount of base promotes aldol condensation between acetaldehyde and FUR to form F2A. In the same way, the increase of conversion also promotes the formation of a higher level of non-detected products since other condensation reactions are also promoted, giving rise to the undesired formation of humins.

Reusability studies were conducted to evaluate the sustainability of the catalysts. For this purpose, the Pd-based catalysts were tested four times at 130 °C for 6 h. The reaction liquid was analyzed and quantified while the solid was filtered, washed with ethanol, and dried to be used in the following test. The catalytic data reported in Figure 10 reveal that all Pd-based catalysts show a decrease in catalytic conversion as the number of cycles increases. After the fourth cycle, the most active catalyst after the 1st cycle (2 wt.% Pd/AC) shows a decrease in conversion from 87% after the first cycle to 40%. However, the catalyst with lower Pd content displays a more progressive deactivation. The highest deactivation of the 2 wt.% Pd/AC catalysts could be related to the formation of a larger amount of non-detected products after each cycle, which could block the available active sites for the oxidation of ethanol to acetaldehyde,[22,23] since the formation of this intermediate seems to be a limiting step in the formation of F2A. This decrease in catalytic activity is reflected in the decay of F2A yield after each cycle, although catalytic deactivation can also be observed with the lower formation of undetected products. Although 2 wt.% Pd/AC catalyst suffers a greater deactivation after 4th cycle, this catalyst still presents the highest conversion and yield toward F2A (25%) after the 4th cycle, probably since this catalyst still maintains higher amount of available Pd-sites on its surface for the oxidation of ethanol to acetaldehyde in comparison to other catalysts.

As the Pd-based catalysts are very prone to deactivation processes, these samples were collected after the fourth cycle to be further characterized to evaluate the possible modification or alteration of the catalysts during the oxidative condensation reaction of FUR.

TEM analysis for the used catalysts (Figures 11 and 12) shows that the Pd nanoparticles maintain the spherical morphology as well as their high dispersion. However, the particle diameter seems to increase slightly in comparison to the Pd-based catalysts before the reaction (Figure 2) due to possible sintering of the Pd nanoparticles under these catalytic conditions. In any case, the average value of the Pd nanoparticles is less than 5 nm in all cases, so the modification of the particle size should hardly affect, to a significant extent, the catalytic deactivation observed.

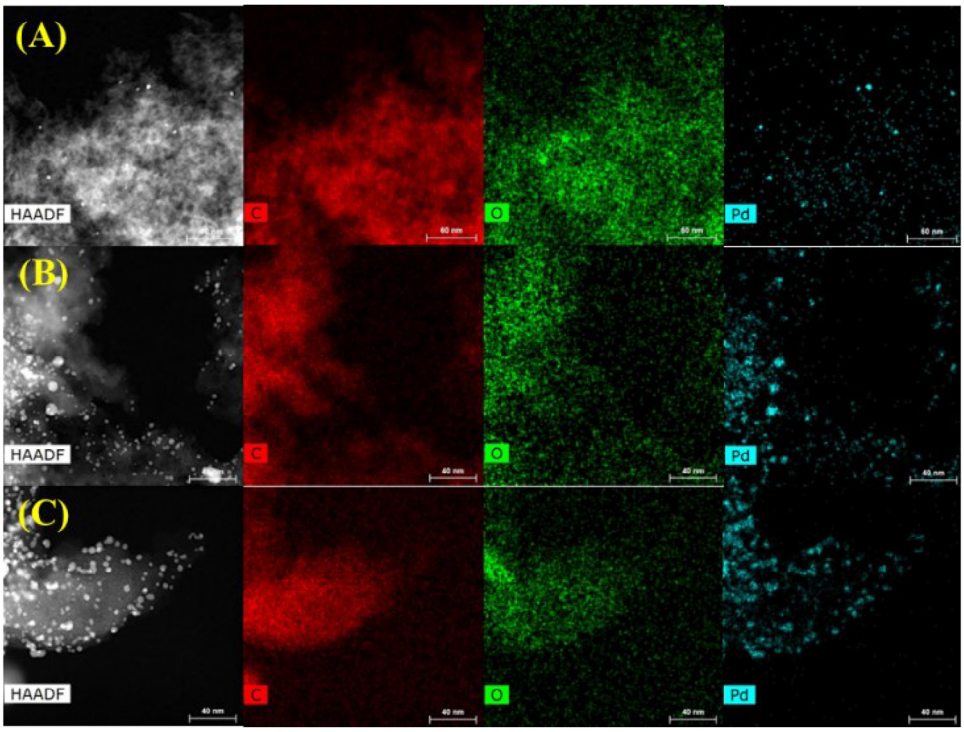

Figure 11. STEM micrographs and elemental analysis of 0.5 wt.% Pd/AC (A), 1 wt.% Pd/AC (B), and 2 wt.% Pd/AC (C) after the reaction. Scale 40 nm. (Experimental conditions: catalyst loading = 0.05 g; amount of FUR = 1 mmol; volume of absolute ethanol = 5 mL; Na_2CO_3 amount = 0–0.10 g; and H_2O_2 (33 vol. %) volume = 0.5 mL; reaction temperature = 130 °C; reaction time = 6 h; number of cycles = 4). Scale 40 nm.

The analysis of the textural properties of the used catalysts (Table 5 and Figure S3, Supporting Information) shows a drastic decrease in the surface area and the microporosity after the reaction for four cycles, decreasing more than five times compared to the starting catalysts (Table 1). Previous studies have reported that the condensation step promotes uncontrolled reactions forming carbonaceous deposits, which seem to block both meso- and micropores, causing a decrease in pore volume such that FUR molecules or products have more limited access.[22,23] On the other hand, the textural properties data indicate that the presence of Pd seems to slightly limit the decay of the surface area and the pore volume.

As the support is an activated carbon with high microporosity, the microporosity of the used catalysts was also studied from the profiles of the CO_2 adsorption isotherms at 0 °C (Table 6 and Figure S4, Supporting Information). As observed in the N_2 isotherms (Table 5), the analysis of the used catalysts reveals that the microporosity determined after four cycles of reaction decreases significantly in comparison to the fresh catalysts (Table 2), confirming a partial blockage of the pores.

The analysis of the chemical composition of the used catalysts on their surface by XPS reveals that the Pd content decreases in all cases (Figure 13 and Table 7), which must be directly related to the deterioration of textural properties (Table 5 and Table 6). Despite the reaction medium is oxidizing, the main contribution after the reaction is attributed to Pd^0. This implies that these species are highly resistant and stable in these reaction conditions. Similarly, surface analysis also reports an increase in carbon content in all catalysts, suggesting the formation of carbonaceous deposits on the surface of the catalyst, which should block, at least partially, the Pd species involved in the reaction, causing a progressive decrease in the catalytic activity (Table 7). In this sense, the formation of these deposits has an adverse effect on the oxidation of ethanol into acetaldehyde. The low proportion of acetaldehyde minimizes the condensation reaction with FUR, leading to a lower amount of F2A when the number of cycles increases. In the same way, the lower activity of the condensation reaction implies the formation of a lower amount of undesired reactions in such a way that the levels of non-detected products are lower, as is shown in Figure 10.

In a final characterization, the modification of the available metallic sites was further evaluated by CO chemisorption (Figure 14). These metallic Pd sites, where CO is chemisorbed, must be involved in the oxidative condensation reaction of ethanol into acetaldehyde. These data reveal a drastic decrease in the adsorption values in comparison to the fresh catalysts. It is striking that all the used catalysts display very similar CO-chemisorption trends regardless of the Pd-loading. The decrease of the CO-chemisorption capacity implies a blocking of these metallic Pd sites, so the oxidation reaction of the alcohol into aldehyde is inhibited. The low proportion of acetaldehyde formed in the oxidation reaction is the limiting step in the oxidative condensation process to form F2A. The blockage of the metallic sites, estimated by CO chemisorption are directly related to the decrease in the textural properties (Table 5 and Table 6) and the decrease of the exposed Pd determined by XPS by the formation of carbonaceous deposits (Figure 13) For all catalysts,

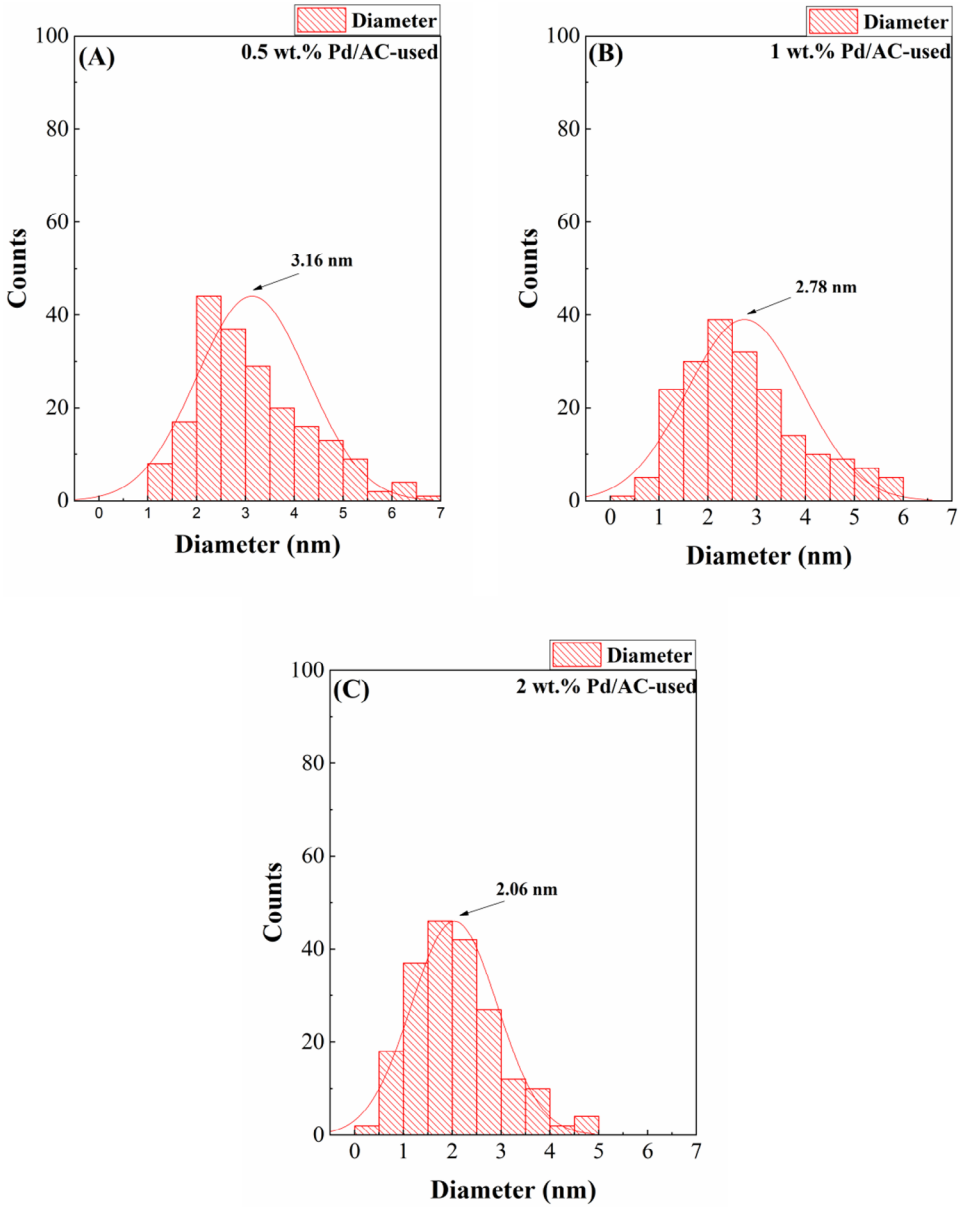

Figure 12. Histograms of the particle diameter for the Pd-species in 0.5 wt.% Pd/AC-used (A), 1 wt.% Pd/AC-used (B) and 2 wt.% Pd/AC-used (C) catalysts after the reaction. Number of measured particles: 200 counts. (Experimental conditions: catalyst loading = 0.05 g; amount of FUR = 1 mmol; volume of absolute ethanol = 5 mL; Na_2CO_3 amount = 0–0.10 g; and H_2O_2 (33 vol. %) volume = 0.5 mL; reaction temperature = 130 °C; reaction time = 6 h; number of cycles = 4).

Table 5. Determination of the textural properties of Pd-based catalysts after the reaction from the N_2 adsorption–desorption isotherms at −196 °C. (Experimental conditions: catalyst loading = 0.05 g; amount of FUR = 1 mmol; volume of absolute ethanol = 5 mL; Na_2CO_3 amount = 0–0.10 g; and H_2O_2 (33 vol. %) volume = 0.5 mL; reaction temperature = 130 °C; reaction time = 6 h; number of cycles = 4).

Catalysts	Langmuir Surface (m^2/g)	t-Plot (m^2/g)	S_{ext}(m^2/g)	Pore Volume (cm^3/g)	Micropore Volume (cm^3/g)
AC-used	144	8	136	0.2498	0.0034
0.5 wt.% Pd /AC-used	169	13	156	0.2634	0.0062
1 wt.% Pd/AC-used	181	8	193	0.2854	0.0037
2 wt.% Pd/AC-used	162	2	160	0.2656	0.0003

Table 6. Determination of the textural properties of Pd-based catalysts after the reaction from the CO_2 adsorption–desorption isotherms at −196 °C. (Experimental conditions: catalyst loading = 0.05 g; amount of FUR = 1 mmol; volume of absolute ethanol = 5 mL; Na_2CO_3 amount = 0–0.10 g; and H_2O_2 (33 vol. %) volume = 0.5 mL; reaction temperature = 130 °C; reaction time = 6 h; number of cycles = 4).

Catalyst	Surface (m^2/g)	Limiting Pore Volume (cm^3/g)
AC used	209	0.0840
0.5 wt.% Pd/AC used	192	0.0772
1 wt.% Pd/AC used	241	0.0967
2 wt.% Pd/AC used	206	0.0825

Table 7. Atomic concentrations on the surface of the catalysts, estimated by of the Pd-based catalysts after the reaction. (Experimental conditions: catalyst loading = 0.05 g; amount of FUR = 1 mmol; volume of absolute ethanol = 5 mL; Na_2CO_3 amount = 0–0.10 g; and H_2O_2 (33 vol. %) volume = 0.5 mL; reaction temperature = 130 °C; reaction time = 6 h; number of cycles = 4).

Catalyst	Atomic Surface Concentrations (%)				
C 1s	O 1s	Pd 3d	Na 1s	Cl 2p	
0.5 wt.% Pd/AC-used	83.48	14.09	0.20	2.01	0.22
1 wt.% Pd/AC-used	82.60	14.75	0.59	1.86	0.20
2 wt.% Pd/AC-used	81.65	15.72	0.95	1.54	0.14

the leaching potential of the Pd-species was analyzed, being less than 1% of its initial content so the catalyst is resistant to the reaction medium.

3. Conclusion

Different amounts of Pd (0.5–2 wt.%) have been deposited on a support with high surface area, such as activated carbon, to study the effect of Pd loading. The methodology described in the present study exhibits high homogeneity of the deposited Pd particles with a small mean particle size (< 5 nm). XPS data indicate that the small Pd particles are mainly in metallic form (Pd^0). This means that the metal particles, which act as the active phase, are widely dispersed and available on their surface to be used as a catalyst.

Once the catalysts were characterized, these materials were tested in the oxidative condensation reaction of FUR to obtain high-added-value products. Catalytic data reveal that the major product is F2A. To obtain this product, an oxidizing agent, such as H_2O_2, is required. Its role is to oxidize the alcohol used in the reaction, that is, ethanol, to obtain acetaldehyde. Once both aldehydes (acetaldehyde and FUR) are present in the reaction medium, a base is required to promote a condensation reaction between them to form F2A. The use of either an oxidizing agent or a base can cause side reactions, which are related to the formation of carbonaceous deposits. On the one hand, FUR is prone to polymerization reactions in an oxidizing medium, while the use of the base can lead to uncontrolled condensation reactions. The analysis of the used catalysts showed that the presence of small Pd particles, including their oxidation state, barely changed. However, XPS analysis revealed an increase in the carbon content on their surfaces, confirming the formation of carbonaceous deposits. In the same way, the XPS spectra also revealed a decrease in the Pd content on the surface, which is directly related to the number of available metal sites, confirming the decay of the conversion and the F2A yield after several cycles.

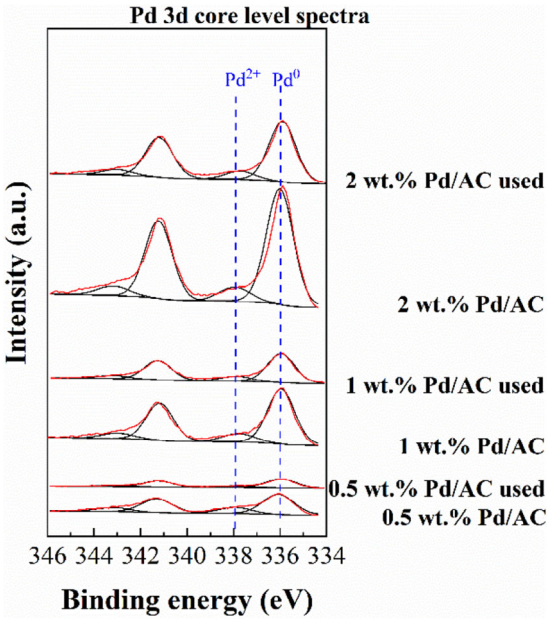

Figure 13. Comparison of the Pd 3d core level spectra before and after the oxidation condensation reaction of FUR. (Experimental conditions: catalyst loading = 0.05 g; amount of FUR = 1 mmol; volume of absolute ethanol = 5 mL; Na_2CO_3 amount = 0–0.10 g; and H_2O_2 (33 vol. %) volume = 0.5 mL; reaction temperature = 130 °C; reaction time = 6 h; number of cycles = 4).

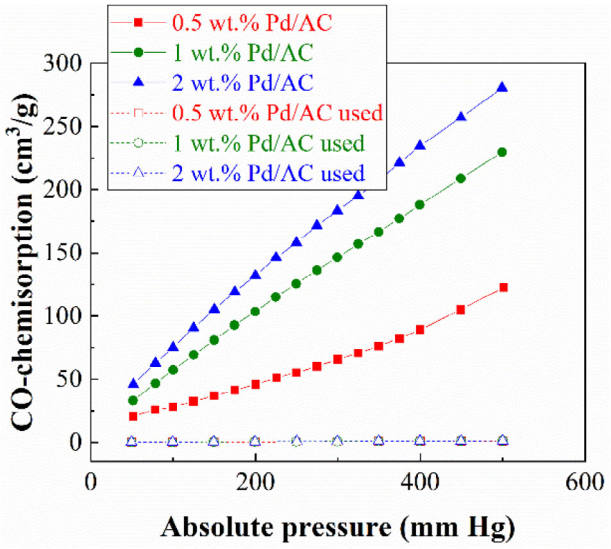

Figure 14. CO-chemisorption of Pd-based catalysts before and after the oxidative condensation reaction of FUR. (Experimental conditions: catalyst loading = 0.05 g; amount of FUR = 1 mmol; volume of absolute ethanol = 5 mL; Na_2CO_3 amount = 0–0.10 g; and H_2O_2 (33 vol. %) volume = 0.5 mL; reaction temperature = 130 °C; reaction time = 6 h; number of cycles = 4).

4. Experimental section

4.1. Materials

The supported Pd catalysts were prepared using a colloidal method.[44] Potassium tetrachloropalladate(II) (Sigma Aldrich, 99.99 %), poly(vinyl alcohol) (PVA, Sigma Aldrich, MW 13,000–23,000 g mol^{-1}, hydrolyzed 87%–89%), sodium borohydride (Sigma Aldrich, powder, ≥98.0%) and activated carbon SX1G (AC, Norit) were used for catalyst preparation. Absolute ethanol (VWR), hydrogen peroxide (VWR, 33% w/v), furfural (Aldrich, 99%), and *o*-xylene (Aldrich, 99.99%) were used for the reaction.

4.2. Catalysts Preparation

A typical experimental protocol is described below for the preparation of the catalysts: 0.031056 g of K_2PdCl_4, corresponding to 0.01 g of Pd metal, was dissolved in 361 mL of distilled water (2.6×10^{-4} M Pd). Then, the desired volume of stabilizer (PVA) solution (0.1010 g/mL) was added. After 3 min, 0.01777 g of sodium borohydride, dissolved in 4.7 mL of water, was added to the solution under stirring ($NaBH_4$:Pd molar ratio = 5:1) to obtain a dark-brown colloidal dispersion. The Pd colloidal solution was stirred for a period of 30 min, and the desired amount of support (0.49, 0.99, and 1.99) was added to the solution to immobilize the Pd-preformed colloidal nanoparticles to obtain three catalysts of 0.5, 1, and 2 wt.% of nominal Pd loading, respectively. The pH of the solution was adjusted to pH = 2 by the addition of concentrated sulfuric acid. The slurry solution was stirred at room temperature for 1 h. Then, the catalyst was filtered using a Buchner funnel. The catalyst was washed several times with distilled water until the filtered aqueous solution reached a pH of 7. Finally, the catalyst was first dried overnight at room temperature, and afterwards it was dried at 80 °C in an oven for 4 h in static air conditions.

4.3. Characterization Techniques

The crystallinity of the supports and catalysts was evaluated by X-ray diffraction (XRD). The morphology of the catalysts and the distribution and size of the Pd particles were analyzed by transmission electron microscopy (TEM). The textural properties of the catalysts were determined from the N_2 adsorption–desorption isotherms at −196 °C, while the microporosity was determined from the CO_2 adsorption–desorption at 0 °C. The Pd content of the catalysts was determined by inductively coupled plasma (ICP) spectrometry. The determination of the metal sites involved in the reaction was carried out from CO chemisorption studies. More detailed information is shown in the Supporting Information file.

4.4. Catalytic Tests

The oxidative condensation reactions were carried out in glass pressure reactors with thread bushing (Ace, 15 mL), which were immersed in an aluminum block under continuous magnetic stirring. The reaction temperature was controlled with a thermocouple immersed inside the aluminum block. For each reaction, 50 mg of Pd-based catalyst was mixed with 1 mmol of FUR (86 µL), 5 mL of absolute ethanol, 0–100 mg of base (Na_2CO_3), 0–0.5 mL of H_2O_2 as oxidant, and 0.02 mL of *o*-xylene, used as internal standard. Once the reactions finished, the reactors were taken out from the aluminum block and immersed in water to stop the reaction. Then, the liquid of the reaction was microfiltered and analyzed by gas chromatography, Shimadzu GC model 14A, which is equipped with a flame ionization detector and a TBR-14 capillary column. FUR conversion and yields were, according to the following equations:

$$\text{Conversion } (\%) = \frac{\text{mol of FUR converved}}{\text{mol of FUR fed}} \times 100$$

$$\text{Yield } (\%) = \frac{\text{mol of product}}{\text{mol of FUR fed}} \times 100$$

Supporting Information

The techniques and equipment used in this work are detailed in the Supporting Information. In the same way, the N_2 and CO_2 adsorption isotherms before and after the reaction are compiled in the Supporting Information (Figures S1–S4).

Acknowledgments

This research was funded by the Spanish Ministry of Science and Innovation (PID2021-122736OB-C42), FEDER (European Union) funds (PID2021-122736OB-C42, UMA20-FEDERJA-088).

Open access publishing facilitated by Universita degli Studi di Bologna, as part of the Wiley - CRUI-CARE agreement.

Conflict of Interests

The authors declare no conflicts of interest.

Data Availability Statement

The data that support the findings of this study are available from the corresponding author upon reasonable request.

Keywords: Furan-2-acrolein · Furfural · Hemicellulose valorization · Oxidative condensation · Pd-nanoparticles

[1] H. J. Brownlee, C. S. Miner, *Ind. Eng. Chem.* **1948**, *40*, 201–204.
[2] Y. Sun, Z. Wang, Y. Liu, X. Meng, J. Qu, C. Liu, B. Qu, *Energies* **2020**,*13*, 21.
[3] K. J. Yong, T. Y. Wu, C. B. T. L. Lee, Z. J. Lee, Q. Liu, J. M. Jahim, Q. Zhou, L. Zhang, *Biomass Bioenergy* **2022**, *161*, 106458.
[4] K. J. Zeitsch, *The chemistry and technology of furfural and its many by-p*, Elsevier Science, Amsterdam **2000**.
[5] K. Yan, G. Wu, T. Lafleur, C. Jarvis, *Renew. Sustain. Energy Rev.* **2014**, *38*, 663–676.
[6] A. Racha, C. Samanta, S. Sreekantan, B. Marimuthu, *Energy Fuels* **2023**, *37*, 11475–11496.
[7] A. O. C. Iroegbu, S. S. Ray, *J. Polym. Sci.* **2024**, *62*, 1044–1060.
[8] P. L. Arias, J. A. Cecilia, I. Gandarias, J. Iglesias, M. López Granados, R. Mariscal, G. Morales, R. Moreno-Tost, P. Maireles-Torres, *Catal. Sci. Technol.* **2020**, *10*, 2721–2757.
[9] Z. Zhang, G. W. Huber, *Chem. Soc. Rev.* **2018**, *47*, 1351–1390.
[10] C. D. Hurd, J. W. Garrett, E. N. Osborne, *J. Am. Chem. Soc.* **1933**, *55*, 1082–1084.
[11] F. Pinna, A. Olivo, V. Trevisan, F. Menegazzo, M. Signoretto, M. Manzoli, F. Boccuzzi, *Catal. Today* **2013**, *203*, 196–201.

[12] F. Menegazzo, M. Signoretto, F. Pinna, M. Manzoli, V. Aina, G. Cerrato, F. Boccuzzi, *J. Catal.* **2014**, *309*, 241–247.
[13] M. Signoretto, F. Menegazzo, L. Contessotto, F. Pinna, M. Manzoli, F. Boccuzzi, *Appl. Catal. B* **2013**, *129*, 287–293.
[14] M. Manzoli, F. Menegazzo, M. Signoretto, D. Marchese, *Catalysts* **2016**, *6*, 107.
[15] D. Yin, Y. Zheng, L. Yang, S. Li, D. Zhu, Y. Guo, C. Zuo, Y. Li, H. Huang, M. Wang, *RSC Adv.* **2021**, *11*, 3280–3287.
[16] W. Yao, C. Hu, Y. Zhang, H. Li, F. Wang, K. Shen, L. Chen, Y. Li, *Ind. Chem. Mater.* **2023**, *1*, 106–116.
[17] X. Tong, Z. Liu, J. Hu, S. Liao, *Appl. Catal. A* **2016**, *510*, 196–203.
[18] E. Monti, A. Ventimiglia, C. A. G. Soto, F. Martelli, E. Rodríguez-Aguado, J. A. Cecilia, P. Maireles-Torres, F. Ospitali, T. Tabanelli, S. Albonetti, F. Cavani, N. Dimitratos, *Mol. Catal.* **2022**, *528*, 112438.
[19] W. Li, M. Gao, B. Qin, X. Deng, L. Li, *Front. Chem. Sci. Eng.* **2024**, *18*, 90.
[20] Z. Liu, X. Tong, J. Liu, S. Xue, *Catal. Sci. Technol.* **2016**, *6*, 1214–1221.
[21] X. Tong, Z. Zhang, Y. Gao, Y. Zhang, L. Yu, Y. Li, *Mol. Catal.* **2019**, *477*, 110545.
[22] J. A. Cecilia, C. P. Jiménez-Gómez, V. Torres-Bujalance, C. García-Sancho, R. Moreno-Tost, P. Maireles-Torres, *Catalysts* **2020**, *10*, 1309.
[23] J. A. Cecilia, L. Machogo, V. Torres-Bujalance, C. P. Jiménez-Gómez, C. García-Sancho, R. Moreno-Tost, P. Maireles-Torres, R. Luque, *ACS Sustainable Chem. Eng.* **2021**, *9*, 10100–10112.
[24] L. Yu, S. Liao, L. Ning, S. Xue, Z. Liu, X. Tong, *ACS Sustainable Chem. Eng.* **2016**, *4*, 1894–1898.
[25] H. Cui, X. Tong, L. Yu, M. Zhang, Y. Yan, X. Zhuang, *Catal. Today* **2019**, *319*, 100–104.
[26] J. Shi, X. Tong, S. Wang, S. Xue, *ACS Catal.* **2022**, *12*, 6029–6035.
[27] X. Tong, L. Yu, X. Luo, X. Zhuang, S. Liao, S. Xue, *Catal. Today* **2017**, *298*, 175–180.
[28] S. Hegde, A. Nizam, A. Vijayan, *New J. Chem.* **2024**, *48*, 1121–1129.
[29] A. Shetty, D. Sunil, T. Rujiralai, S. P. Maradur, A. N. Alodhayb, G. Hegde, *Nanoscale Adv.* **2024**, *6*, 2516–2526.
[30] K. Yang, M. Chen, C. Liu, X. Lin, D. Hou, Y. Zheng, H. Sun, F. Yang, J. Z. Sun, *ACS Appl. Nano Mater.* **2025**, *8*, 3064–3072.
[31] Z. Q. Li, C. J. Lu, Z. P. Xia, Y. Zhou, Z. Luo, *Carbon* **2007**, *45*, 1686–1695.
[32] M. Thommes, K. Kaneko, A. V. Neimark, J. P. Olivier, F. Rodriguez-Reinoso, J. Rouquerol, K. S. W. Sing, *Pure Appl. Chem.* **2015**, *87*, 1051–1069.
[33] D. Lozano-Castelló, D. Cazorla-Amorós, A. Linares-Solano, *Carbon* **2004**, *42*, 1233–1242.
[34] A. Dantas, K. C. Struckhoff, M. Thommes, A. V. Neimark, *Carbon* **2021**, *173*, 842–848.
[35] M. M. Dubinin, *Carbon* **1989**, *27*, 457–467.
[36] J. F. Moulder, W. F. Stickle, P. E. Sobol, K. D. Bomben, *Handbook of X-Ray Photoelectron Spectroscopy*, Perkin-Elmer, Eden Praire, Minnesota, USA **1992**.
[37] L. Ning, S. Liao, X. Liu, P. Guo, Z. Zhang, H. Zhang, X. Tong, *J. Catal.* **2018**, *364*, 1–13.
[38] M. J. Ndolomingo, N. Bingwa, R. Meijboom, *J. Mater. Sci.* **2020**, *55*, 6195–6241.
[39] V. Torres-Bujalance, J. A. Cecilia, C. García-Sancho, F. J. García-Mateos, J. M. Rosas, R. Moreno-Tost, J. Rodríguez-Mirasol, T. Cordero, P. Maireles-Torres, *Renew. Energy* **2024**, *221*, 119772.
[40] Q. Fang, Z. Qin, Y. Shi, F. Liu, S. Barkaoui, H. Abroshan, G. Li, *ACS Appl. Energy Mater.* **2019**, *2*, 2654–2661.
[41] P. Devendar, R. Y. Qu, W. M. Kang, B. He, G. F. Yang, *J. Agric. Food Chem.* **2018**, *66*, 8914–8934.
[42] R. M. Mironenko, O. B. Belskaya, V. P. Talsi, V. A. Likholobov, *J. Catal.* **2020**, *389*, 721–734.
[43] R. Šivec, M. Huš, B. Likozar, M.i. Grilc, *Chem. Eng. J.* **2022**, *436*, 135070.
[44] S. Scurti, E. Monti, E. Rodríguez-Aguado, D. Caretti, J. A. Cecilia, N. Dimitratos, *Nanomaterials* **2021**, *11*, 879–897.

Manuscript received: March 30, 2025
Revised manuscript received: June 11, 2025
Accepted manuscript online: June 11, 2025
Version of record online: July 3, 2025